Signature of Collective Plasma Effects in Beam-Driven QED Cascades

Kenan Qu[1], Sebastian Meuren[1,2] and Nathaniel J. Fisch[1]

[1]*Department of Astrophysical Sciences, Princeton University, Princeton, New Jersey 08544, USA*
[2]*Stanford PULSE Institute, SLAC National Accelerator Laboratory, Menlo Park, California 94025, USA*

QED cascades play an important role in extreme astrophysical environments like magnetars. They can also be produced by passing a relativistic electron beam through an intense laser field. Signatures of collective pair plasma effects in these QED cascades are shown to appear, in exquisite detail, through plasma-induced frequency upshifts in the laser spectrum. Remarkably, these signatures can be detected even in small plasma volumes moving at relativistic speeds. Strong-field quantum and collective pair plasma effects can thus be explored with existing technology, provided that ultradense electron beams are colocated with multipetawatt lasers.

Introduction.—Intriguing astrophysical environments like magnetars [1–13], binary neutron-star mergers [14,15], and core-collapse supernovae explosions [16,17] exhibit magnetic fields substantially exceeding the QED critical field, also known as the Schwinger field [18]. Strong-field QED cascades fill these astrophysical objects with high-density relativistic electron-positron pairs [19–26] such that plasma effects become important. However, the interplay between strong-field quantum and collective plasma effects in what might be called the "QED plasma regime" remains poorly understood [27–30].

There is thus strong motivation to elucidate the physics of QED plasmas in laboratory experiments. Even though they cannot reproduce magnetar-strength magnetic fields, the Lorentz boost of ultrarelativistic particles allows us to probe analogous conditions and produce a beam-driven QED cascade with exponentially growing electron, positron, and photon densities (see Supplemental Material [31]). Such an experiment is possible only when the critical field is significantly exceeded in the boosted frame [42] and quantum corrections to synchrotron emission and pair production become important [43–54]. The QED cascade then might generate pairs at a density high enough that collective plasma effects begin to play a large role.

We show that, in fact, the combination of a 3 PW laser and a *dense* 30 GeV electron beam produces a quasineutral pair plasma with a density that is comparable to the critical one. Such laser systems are routinely operated in several laboratories [55]. An electron beam with 10 GeV energy and 3×10^{19} cm^{-3} peak density represents the state of the art, available at the FACET-II facility [56]. The electron beam parameters assumed here (30 GeV energy, 4×10^{20} cm^{-3} density) could be achieved at SLAC with a new bunch compressor by combining the FACET-II and LCLS-Cu linac [42,57,58].

This beam-laser collision approach has three significant advantages over the all-optical laser-laser collision approach. First, in producing the pair plasma, the required laser intensity (3×10^{22} W cm^{-2}) and laser power (a few petawatt) are far lower than those of the all-optical approach, which requires intensities above 10^{24} W cm^{-2} [59–70], only available at large 100PW-scale laser facilities [71–73]. Second, and very importantly, not only is the QED plasma regime easier to produce, but it is easier to observe once it is produced. Because the intensities are lower, the average gamma factor of the produced pair plasma is also much lower. This means that, at the same pair density, the plasma frequency, which signifies collective effects, is much higher. The beam-laser approach thus solves the coupled production-observation problem. Third, seeding the cascade with a beam instead of a gaseous or solid target results in a high degree of experimental control.

In fact, the QED plasma regime is notoriously hard to observe, both in seeded laser-laser and beam-laser collisions. The plasma is moving and expanding at relativistic speeds and its volume is similar or smaller than the skin depth for realistic laser parameters. Conventional detection methods, e.g., by observing plasma instabilities like the two-stream instability [74], the Weibel instability [75], or stimulated Brillouin scattering [76], become very difficult or even impossible with such small plasma volumes. Exploring the QED plasma regime with existing technology therefore requires a new kind of diagnostic.

We show here that frequency upshifts in the laser spectrum inform importantly and in exquisite detail on the interplay between strong-field quantum and collective plasma effects. They are induced by the time-varying pair plasma density, both as it forms and as it radiates. A frequency upshift or downshift occurs whenever the index of refraction changes suddenly [77–84]. Here, pair

production changes the particle density and thus the plasma frequency. In addition, quantum synchrotron radiation reduces the electron and positron energy, and hence their effective masses, which also increases the plasma frequency. As we show, both analytically and numerically, detailed signatures of these effects appear in the output laser field spectrum, which are measurable at intensities as low as 10^{22} W cm^{-2}.

Thus, remarkably, despite the small plasma volume and despite the relativistic plasma motion, signatures of the QED plasma regime might be identified experimentally with state-of-the-art technology. What emerges is a compelling argument for colocating laser and beam facilities to explore QED cascades, in general, and the QED plasma regime, in particular.

Frequency upshift.—When electron-positron pairs are generated in a strong laser field, their oscillation reduces the optical permittivity, thereby upshifting the laser frequency. The frequency upshift is determined by the collective plasma parameter, i.e., the plasma frequency [85] $\omega_p = \sqrt{2n_p e^2/(\gamma m_e \varepsilon_0)}$. Here, $2n_p$ is the total density of the pair particles, $e > 0$ is the elementary charge, ε_0 is the vacuum permittivity, m_e is the electron-positron rest mass, and γ is the Lorentz factor. If a small volume, counterpropagating plasma is created, it changes the instantaneous laser frequency and wave vector by [31,77,86,87]

$$\Delta\omega(x,t) = \omega_0 \int_{t_0}^{t} dt' \left[\frac{\partial}{\partial T} \frac{n_p(X,T)}{n_c \gamma(X,T)} \right]_{X=x-c(t-t')}^{T=t'}, \quad (1)$$

$$\Delta k(x,t) = \Delta\omega(x,t)/c - \omega_p^2(x,t)/(2\omega_0 c), \quad (2)$$

where ω_0 is the input laser frequency, and n_c is the corresponding critical plasma density defined as $\omega_0^2 = e^2 n_c/(m_e \varepsilon_0)$. After the plasma traverses through the laser, $\Delta\omega$ becomes asymptotically identical to $c\Delta k$. According to Eq. (1), the maximum frequency upshift is $\Delta\omega/\omega_0 \approx n_p/(n_c\gamma)$. Although frequency up-conversion also reduces the laser intensity and changes the laser polarization [78,83], experimental detection of these secondary effects is more challenging than measuring the laser frequency shift.

Pair plasma generation.—An electron beam colliding with a laser pulse induces a QED cascade during the ramp-up of laser intensity as soon as the local quantum parameter $\chi_e \equiv E^*/E_s \gtrsim 1$. Here, $E_s = m_e^2 c^3/(\hbar e) \approx 1.3 \times 10^{18}$ V m^{-1} is the critical field, and $E^* = \gamma|\mathbf{E}_\perp + \boldsymbol{\beta} \times c\mathbf{B}|$ is the electric field measured in the electron rest frame; $\mathbf{E}$ and $\mathbf{B}$ are the laser electric field and magnetic field in the laboratory frame, $\boldsymbol{\beta}$ is the electron velocity normalized to the speed of light c, and $\gamma = (1-\boldsymbol{\beta}^2)^{-1/2}$.

Depending on the field configuration, the effective expression for χ_e changes, but the dependence of, e.g., the pair production and the photon emission probability on
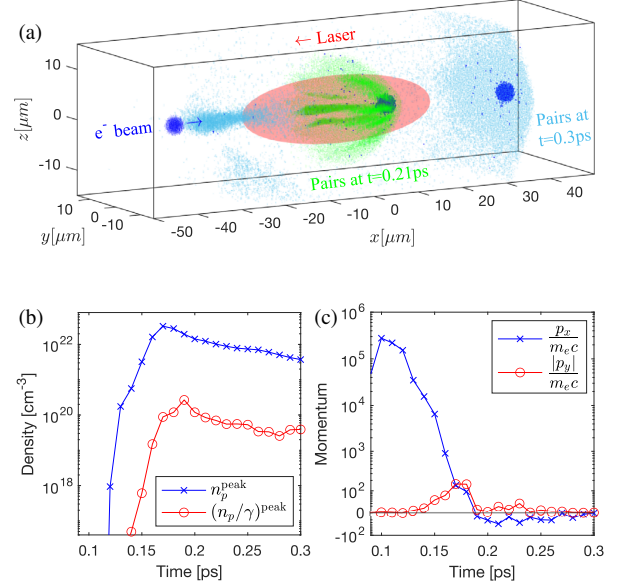

FIG. 1. (a) 3D PIC simulation of a beam-driven QED cascade. An energetic, high-density electron beam (deep blue) collides with a multipetawatt laser pulse (yellow), creating an electron-positron pair plasma through a QED cascade. The pair plasma is shown at $t = 0.21$ ps (green) and $t = 0.3$ ps (light blue). (b) Evolution of peak pair plasma density n_p (blue) and the parameter n_p/γ (red), which determines the laser frequency upshift. (c) Evolution of pair particle momenta in longitudinal (blue) and transverse (red) directions, normalized to $m_e c$.

χ_e remains universal for ultrarelativistic particles. Therefore, a laboratory experiment can provide insights relevant for extreme astrophysical plasmas, e.g., those encountered in close proximity to magnetars.

During the collision, the pair density continues to grow until either the beam and/or laser energy is depleted or the laser intensity ramps down. For an electron beam with energy $\gamma_0 m_e c^2$ and a laser with dimensionless amplitude $a_0 \equiv eE/(m_e c\omega_0)$ the quantum parameter could reach a maximum value of $\tilde{\chi}_e \approx 2a_0\gamma_0(\hbar\omega_0)/(m_e c^2)$. Since each particle with $\chi_e \gtrsim 1$ continues to create new pairs, the final pair density scales with $n_p \sim \tilde{\chi}_e n_e$, although practical constraints like the finiteness of the interaction volume and the interaction time can cause deviations from this simple relation.

To show how a dense electron beam can indeed probe the QED plasma regime, where collective effects induce a laser frequency upshift, we carried out a "proof-of-principle" 3D numerical simulation with the state-of-the-art particle-in-cell (PIC) code EPOCH [88,89] that provides a QED module (see, e.g., [52,64,70,90]). To illustrate the effect, we consider a 1 nC, 300 GeV electron beam [91,92], shown as a blue sphere in Fig. 1(a), which collides with a counterpropagating 0.8 μm wavelength, 24 PW laser pulse
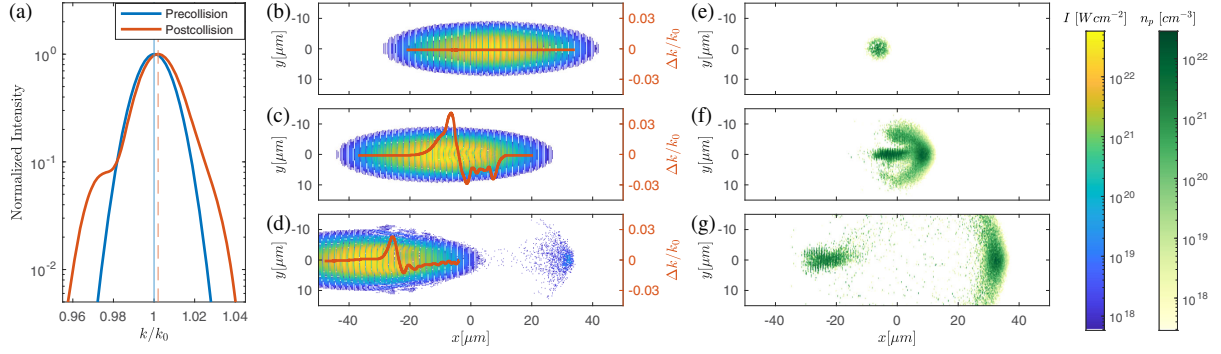
FIG. 2. (a) Normalized laser intensity spectra of wave numbers before and after the laser pulse–electron beam collision. The thin vertical lines show the peak positions. Snapshots at (b),(e) $t = 0.15$ ps, (c),(f) $t = 0.2$ ps, and (d),(g) $t = 0.28$ ps. The pseudocolor plots (b)–(d) show the laser beam profiles at $z = 0$. The red curve represents the instantaneous laser wave number through a synchrosqueezed wavelet transform of the laser field at $y = z = 0$. The plots (e)–(g) show the pair density at $z = 0$.

[72], shown as an yellow spheroid (see Supplemental Material [31]). The effect is shown in detail in the 3D simulation; it can also be observed with less extreme conditions, though the exact upshifts are harder to resolve numerically.

The electron beam sphere is injected from the left boundary ($x = -50\ \mu$m) with a density distribution $n_e = n_0 \exp\{-[(x + 50\ \mu\text{m} - ct)^2 + \rho^2]/(2r_0^2)\}$, where $\rho = \sqrt{y^2 + z^2}$, $n_0 = 4 \times 10^{20}$ cm^{-3}, and $r_0 = 1\ \mu$m. The Gaussian laser pulse with linear y polarization is injected from the right boundary to focus at the central plane $x = 0$. The laser intensity profile is $I \simeq I_0 \cdot [w_0/w(x)]^2 \times \exp[-2\rho^2/w^2(x)] \exp[-2(x - 48\ \mu\text{m} + ct)^2/\tau^2]$, where $I_0 = 6 \times 10^{22}$ W cm^{-2} is the peak intensity, $w(x) = w_0\sqrt{1 + (x/x_R)^2}$, $x_R = \pi w_0^2/\lambda \simeq 98\ \mu$m is the Rayleigh length, $w_0 = 5\ \mu$m is the waist, and $\tau = 50$ fs is the pulse duration. If the electron beam energy was not depleted by the QED cascade, these parameters would yield a quantum parameter $\tilde{\chi}_e \approx 220$ at the Gaussian waist in the focal plane and $\tilde{\chi}_e \approx 600$ at the laser focus. The simulation starts at $t = -0.205$ ps and ends at 0.32 ps.

The simulation shows that the collision quickly creates a pair plasma with an exponentially growing density, as illustrated in Fig. 1(b). The 2D cross section plots in Figs. 2(e)–2(g) show a balloonlike plasma expansion caused by a transverse acceleration of the pairs in the strong laser field. The pairs are principally located near the core of the electron beam, and only a small amount of low-energy pairs expands in the strong laser field. The peak plasma density, shown as a blue curve in Fig. 1(b), reaches a peak value of $n_p = 82n_0 = 3.3 \times 10^{22}$ cm^{-3} at $t = 0.17$ ps. At the same time, the total charge saturates at a peak value of $139nC$. The laterally expanding particles move to regions with lower laser intensity and even leave the simulation box.

Plasma deceleration.—The parameter n_p/γ, which determines the frequency upshift, continues to grow even

after the pair density n_p reaches its peak value. This implies that γ decreases faster than n_p until $t = 0.19$ ps, where n_p/γ reaches the peak value 2.7×10^{20} cm^{-3}.

While pair generation happens when the particle quantum parameter $\chi_e \gtrsim 1$, pairs with $\chi_e \lesssim 1$ continue to lose energy via synchrotron radiation. The energy loss remains significant as long as $\chi_e \gtrsim 0.1$. Thus, in a sufficiently long laser pulse, the laser reduces the pair gamma factor asymptotically to

$$\gamma \lesssim 0.1 \frac{\gamma_0}{\tilde{\chi}_e} \approx \frac{0.05}{a_0} \frac{m_e c^2}{\hbar\omega_0}. \tag{3}$$

The effect of radiation friction is shown in Fig. 1(c), where the blue curve reveals that the pair plasma rapidly loses longitudinal momentum before $t = 0.19$ ps.

Particle reflection.—According to the classical equations of motions the radiation pressure of a counter-propagating plane-wave laser field can (instantaneously) transfer energy of the order of $m_e c[a_0^2/(4\gamma)]$ [43]. If the symmetry of acceleration/deceleration is broken, e.g., by the emission of photons which induce a large recoil, the laser can stop and even reflect electrons/positrons [93,94]. As a result, Eq. (3) is only valid until $\gamma \sim a_0$, at which point the plasma is reflected and re-accelerated by the counter-propagating laser. Thus, we find that particle reflection is possible if

$$a_0 \gtrsim \sqrt{0.05 m_e c^2/(\hbar\omega_0)}, \tag{4}$$

for a sufficiently long laser pulse. For optical lasers with $\hbar\omega_0 \sim 1$ eV, the threshold is approximately $a_0 \gtrsim 100$, corresponding to $I \gtrsim 10^{22}$–10^{23} W cm^{-2}. Reflection of the plasma can be observed in Fig. 1(c) and Fig. 2(g): the longitudinal momentum becomes negative at $t = 0.2$ ps and the pairs are spreading throughout the simulation box at $t = 0.3$ ps.

Particle reflection is critically advantageous, because the maximum laser frequency upshift is induced when the plasma gamma factor reaches its minimum. Hence, we can assume $\gamma \sim a_0$ for the plasma gamma factor. Figure 1(c) shows that the maximum transverse momentum is $\sim a_0 m_e c$. Thus, one obtains the following rule of thumb for the maximum achievable pair plasma density and the relevant gamma factor

$$n_p \sim \tilde{\chi}_e n_e, \quad \gamma \sim a_0, \qquad (5)$$

if the condition given in Eq. (4) is met and the QED cascade reaches its asymptotic state.

Scaling laws.—By combining Eq. (1) with Eq. (5), one finds an order-of-magnitude estimate for the expected laser frequency upshift

$$\frac{\omega_f^2}{\omega_0^2} - 1 \sim \frac{\tilde{\chi}_e n_e}{n_c a_0} \sim \gamma_0 \frac{\hbar \omega_0}{m_e c^2} \frac{n_e}{n_c}. \qquad (6)$$

This relation is valid for an idealized model, i.e., a homogeneous electron beam counterpropagating with a plane-wave laser. It assumes that the QED cascade fully develops and that the pair plasma is eventually stopped and reflected.

The simulation shown in Fig. 1 yields a pair plasma that has a peak value of n_p/γ corresponding to 6.7% of the critical plasma density at rest $n_c \approx 1.7 \times 10^{21}$ cm^{-3}. A possible experimental setup uses two on-axis parabolic mirrors with a hole to focus and recollect the laser. On the axis $y = z = 0$, where we have the highest numerical resolution, the Fourier-transformed electric field, shown in Fig. 2(a), reveals an upshift of the peak wave vector by $\Delta k/k_0 \approx 0.2\%$. We also see an excess of up- and down-shifted photons around $\Delta k/k_0 \approx \pm 5\%$. A change of this order of magnitude is expected based on Eq. (2) and the peak plasma density observed in Fig. 1(b). The change of wave vector transforms into a change of frequency when the plasma exits the laser pulse.

A more sophisticated time-frequency analysis based on wavelet transforms [95–97] is shown in Figs. 2(b)–2(d). Such a time-frequency diagram could be measured with techniques like frequency-resolved optical gating [98] or spectral shear interferometry for direct electric field reconstruction [99]. The numerical analysis shows that the flattop input frequency spectrum [see Fig. 2(b)] becomes chirped at the region of plasma creation near $x = 0$ in Fig. 2(c). The chirped region propagates along the laser direction. The maximum instantaneous wave vector upshift reaches $\Delta k/k_0 \approx 2.4\%$. This amount of up- and downshift is in agreement with the up- and downshift observed in the front and tail of the Fourier spectrum in Fig. 2(a).

Parameter scan.—To verify the analytical scaling laws given above, a series of 1D QED-PIC simulations were
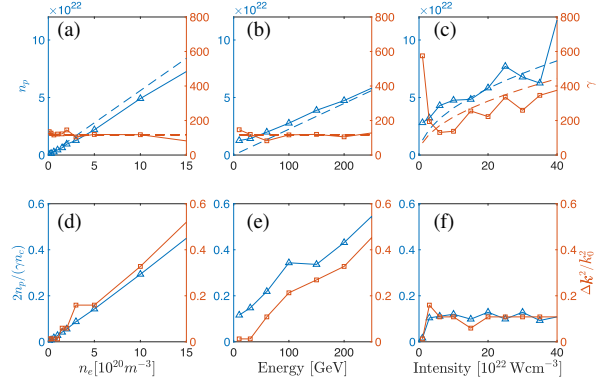

FIG. 3. (a)–(c) The peak density n_p and the Lorentz factor γ of the created pair plasma. (d)–(f) Analytical predictions and numerically simulated peak values of the relative frequency upshift of the laser pulse. The numerical 1D PIC simulations (marked curves) employ $n_e = 4 \times 10^{19}$ cm^{-3} peak electron beam density [except in (a) and (d)], 1 $\mu m/c$ rms duration, 100 GeV energy [except in (b) and (e)]; 3×10^{22} W cm^{-2} laser peak intensity [except in (d) and (f)], and 100 fs pulse duration. The dashed curves show the theoretical estimates from Eqs. (5) and (1), respectively.

conducted with different electron beam densities, beam energies, and laser intensities. These parameter scans are possible, as 1D simulations require significantly less computational resources. They do not model transverse effects such as plasma inhomogeneity and laser diffraction, but the particle momenta and currents, which are responsible for the plasma permittivity, and hence the laser frequency upshift, are effectively simulated in three dimensions.

Figures 3(a) and 3(b) show that either increasing the beam density or the beam energy causes a linear increase of the created pair plasma density, whereas the final gamma factor remains constant at about $\gamma \approx a_0$. Both observations are in agreement with Eq. (5). The maximum frequency upshift shown in Figs. 3(d) and 3(e) shows a linear scaling in decent agreement with Eq. (6). When the laser intensity I is increased in Figs. 3(c) and 3(f), both plasma density n_p and gamma factor γ increase as $\sqrt{I}$ [see Eq. (5)]. The parameter n_p/γ remains constant, implying that the laser frequency upshift is independent of the laser intensity I as long as the particle reflection condition [see Eq. (4)] is met. The reflection condition is violated for laser intensities below 3×10^{22} W cm^{-2}, causing a deviation of the frequency upshift from this scaling at very low intensities.

According to Eq. (6) and Fig. 3, a laser frequency upshift, reflecting collective effects, becomes observable experimentally if the laser intensity and electron beam density are above $\sim 10^{22}$ W cm^{-2} and $\sim 10^{20}$ cm^{-3}, respectively. Such parameters require only a moderate upgrade of existing facilities, e.g., SLAC's FACET-II [56]. Indeed, a separate set of 3D QED-PIC simulations shows the

tantalizing prospect: a 3 PW laser pulse (50 fs duration, 2.5 μm waist, 3×10^{22} W cm^{-2} intensity), colliding with a 1 nC, 30 GeV, 4×10^{20} cm^{-3} electron beam creates an electron-positron pair plasma of 19 nC and peak density of 5×10^{21} cm^{-3}. It causes 0.5% maximum local frequency changes after the collision. While 3D-PIC simulations were not able to resolve the central frequency shift of the whole laser pulse (due to limitations of computing resources), it clearly follows that an experimental measurement of the laser frequency upshift would be feasible for these parameters.

Interestingly, the produced pair plasma also exhibits many other collective plasma effects once the parameter n_p/γ exceeds the critical density. For example, plasma filamentation can be observed in Figs. 1(a) and 2(f), possibly arising from the Weibel instability [75].

Conclusion.—A beam-laser collision setup, together with a method of observation, solves the very challenging joint problem of both producing and observing the QED plasma regime. Moreover, this joint problem is solved using existing state-of-the-art beam and laser facilities, which argues compellingly for their colocation. A key feature in this solution was to limit the pair plasma energy, thereby to increase its role in collective effects. Providing access to the QED plasma regime with available technology now offers the very real possibility to study in the laboratory the high-energy density physics relevant to some of the very recently uncovered and most enigmatic phenomena in astrophysics.

---

[1] V. M. Kaspi and A. M. Beloborodov, Magnetars, Annu. Rev. Astron. Astrophys. **55,** 261 (2017).

[2] B. Cerutti and A. M. Beloborodov, Electrodynamics of pulsar magnetospheres, Space Sci. Rev. **207,** 111 (2017).

[3] L. Lin, C. F. Zhang, P. Wang et al., No pulsed radio emission during a bursting phase of a Galactic magnetar, Nature (London) **587,** 63 (2020).

[4] A. Ridnaia, D. Svinkin, D. Frederiks, A. Bykov, S. Popov, R. Aptekar, S. Golenetskii, A. Lysenko, A. Tsvetkova, M. Ulanov, and T. L. Cline, A peculiar hard x-ray counterpart of a galactic fast radio burst, Nat. Astron. **5,** 372 (2021).

[5] C. K. Li, L. Lin, S. L. Xiong et al., HXMT identification of a non-thermal x-ray burst from SGR J1935+2154 and with FRB 200428, Nat. Astron. **5,** 378 (2021).

[6] C. D. Bochenek, V. Ravi, K. V. Belov, G. Hallinan, J. Kocz, S. R. Kulkarni, and D. L. McKenna, A fast radio burst associated with a galactic magnetar, Nature (London) **587,** 59 (2020).

[7] B. C. Andersen, K. M. Bandura, M. Bhardwaj et al., A bright millisecond-duration radio burst from a galactic magnetar, Nature (London) **587,** 54 (2020).

[8] B. Marcote, K. Nimmo, J. W. T. Hessels et al., A repeating fast radio burst source localized to a nearby spiral galaxy, Nature (London) **577,** 190 (2020).

[9] CHIME/FRB Collaboration, A second source of repeating fast radio bursts, Nature (London) **566,** 235 (2019).

[10] V. Ravi, M. Catha, L. D'Addario, S. G. Djorgovski, G. Hallinan, R. Hobbs, J. Kocz, S. R. Kulkarni, J. Shi, H. K. Vedantham, S. Weinreb, and D. P. Woody, A fast radio burst localized to a massive galaxy, Nature (London) **572,** 352 (2019).

[11] K. W. Bannister, A. T. Deller, C. Phillips et al., A single fast radio burst localized to a massive galaxy at cosmological distance, Science **365,** 565 (2019).

[12] J. M. Cordes and S. Chatterjee, Fast radio bursts: An extragalactic enigma, Annu. Rev. Astron. Astrophys. **57,** 417 (2019).

[13] E. Petroff, J. W. T. Hessels, and D. R. Lorimer, Fast radio bursts, Astron. Astrophys. Rev. **27,** 4 (2019).

[14] Y. Q. Xue, X. C. Zheng, Y. Li et al., A magnetar-powered x-ray transient as the aftermath of a binary neutron-star merger, Nature (London) **568,** 198 (2019).

[15] D. J. Price and S. Rosswog, Producing ultrastrong magnetic fields in neutron star mergers, Science **312,** 719 (2006).

[16] P. Mösta, C. D. Ott, D. Radice, L. F. Roberts, E. Schnetter, and R. Haas, A large-scale dynamo and magnetoturbulence in rapidly rotating core-collapse supernovae, Nature (London) **528,** 376 (2015).

[17] S. Akiyama, J. Craig Wheeler, D. L. Meier, and I. Lichtenstadt, The magnetorotational instability in core-c supernova explosions, Astrophys. J. **584,** 954 (2003).

[18] J. Schwinger, On gauge invariance and vacuum polarization, Phys. Rev. **82,** 664 (1951).

[19] A. Y. Chen, F. Cruz, and A. Spitkovsky, Filling the magnetospheres of weak pulsars, Astrophys. J. **889,** 69 (2020).

[20] A. N. Timokhin and A. K. Harding, On the maximum pair multiplicity of pulsar cascades, Astrophys. J. **871,** 12 (2019).

[21] R. Gueroult, Y. Shi, J.-M. Rax, and N. J. Fisch, Determining the rotation direction in pulsars, Nat. Commun. **10,** 3232 (2019).

[22] M.-H. Wang, S.-K. Ai, Z.-X. Li, N. Xing, H. Gao, and B. Zhang, Testing the hypothesis of a compact-binary-coalescence origin of fast radio bursts using a multimessenger approach, Astrophys. J. **891,** L39 (2020).

[23] B. P. Abbott, R. Abbott, T. D. Abbott et al., GW190425: Observation of a compact binary coalescence with total mass ~3.4 $M_\odot$, Astrophys. J. **892,** L3 (2020).

[24] LIGO Scientific Collaboration and Virgo Collaboration, GW170817: Observation of Gravitational Waves from a Binary Neutron Star Inspiral, Phys. Rev. Lett. **119,** 161101 (2017).

[25] C. Palenzuela, L. Lehner, M. Ponce, S. L. Liebling, M. Anderson, D. Neilsen, and P. Motl, Electromagnetic and Gravitational Outputs from Binary-Neutron-Star Coalescence, Phys. Rev. Lett. **111**, 061105 (2013).

[26] M. Anderson, E. W. Hirschmann, L. Lehner, S. L. Liebling, P. M. Motl, D. Neilsen, C. Palenzuela, and J. E. Tohline, Magnetized Neutron-Star Mergers and Gravitational-Wave Signals, Phys. Rev. Lett. **100**, 191101 (2008).

[27] D. B. Melrose and R. Yuen, Pulsar electrodynamics: An unsolved problem, J. Plasma Phys. **82**, 635820202 (2016).

[28] D. A. Uzdensky and S. Rightley, Plasma physics of extreme astrophysical environments, Rep. Prog. Phys. **77**, 036902 (2014).

[29] D. Uzdensky, M. Begelman, A. Beloborodov *et al.*, Extreme plasma astrophysics, arXiv:1903.05328.

[30] P. Zhang, S. S. Bulanov, D. Seipt, A. V. Arefiev, and A. G. R. Thomas, Relativistic plasma physics in supercritical fields, Phys. Plasmas **27**, 050601 (2020).

[31] See Supplemental Material at http://link.aps.org/supplemental/10.1103/PhysRevLett.127.095001 for its relation to astrophysical plasmas and for more details on the theory and numerical simulations, which includes Refs. [32–41].

[32] V. B. Berestetskii, E. M. Lifshitz, and L. P. Pitaevskii, *Quantum Electrodynamics*, 2nd ed. (Butterworth-Heinemann, Washington, DC, 1982).

[33] S. A. Olausen and V. M. Kaspi, The McGill magnetar catalog, Astrophys. J. Suppl. **212**, 6 (2014).

[34] J. D. Jackson, *Classical Electrodynamics*, 3rd ed. (Wiley, New York, NY, 1999).

[35] B. Cros, Laser-driven plasma wakefield: Propagation effects, Technical Report, CERN Yellow Reports, 2016, https://doi.org/10.5170/CERN-2016-001.207.

[36] T. Erber, High-energy electromagnetic conversion processes in intense magnetic fields, Rev. Mod. Phys. **38**, 626 (1966).

[37] Y. I. Salamin, G. R. Mocken, and C. H. Keitel, Electron scattering and acceleration by a tightly focused laser beam, Phys. Rev. ST Accel. Beams **5**, 101301 (2002).

[38] V. I. Ritus, Quantum effects of the interaction of elementary particles with an intense electromagnetic field, J. Sov. Laser Res. **6**, 497 (1985).

[39] S. Meuren, K. Z. Hatsagortsyan, C. H. Keitel, and A. Di Piazza, Polarization-operator approach to pair creation in short laser pulses, Phys. Rev. D **91**, 013009 (2015).

[40] *NIST Handbook of Mathematical Functions*, edited by F. W. J. Olver, D. W. Lozier, R. F. Boisvert, and C. W. Clark (Cambridge University Press, Cambridge, England, 2010).

[41] S. W. Smith, *The Scientist and Engineer's Guide to Digital Signal Processing*, 2nd ed. (California Technical Publishing, San Diego, 1999).

[42] V. Yakimenko, S. Meuren, F. Del Gaudio *et al.*, Prospect of Studying Nonperturbative QED with Beam-Beam Collisions, Phys. Rev. Lett. **122**, 190404 (2019).

[43] A. Di Piazza, C. Müller, K. Z. Hatsagortsyan, and C. H. Keitel, Extremely high-intensity laser interactions with fundamental quantum systems, Rev. Mod. Phys. **84**, 1177 (2012).

[44] I. V. Sokolov, N. M. Naumova, J. A. Nees, and G. A. Mourou, Pair Creation in QED-Strong Pulsed Laser Fields

Interacting with Electron Beams, Phys. Rev. Lett. **105**, 195005 (2010).

[45] H. Hu, C. Müller, and C. H. Keitel, Complete QED Theory of Multiphoton Trident Pair Production in Strong Laser Fields, Phys. Rev. Lett. **105**, 080401 (2010).

[46] A. G. R. Thomas, C. P. Ridgers, S. S. Bulanov, B. J. Griffin, and S. P. D. Mangles, Strong Radiation-Damping Effects in a Gamma-Ray Source Generated by the Interaction of a High-Intensity Laser with a Wakefield-Accelerated Electron Beam, Phys. Rev. X **2**, 041004 (2012).

[47] N. Neitz and A. Di Piazza, Stochasticity Effects in Quantum Radiation Reaction, Phys. Rev. Lett. **111**, 054802 (2013).

[48] S. S. Bulanov, C. B. Schroeder, E. Esarey, and W. P. Leemans, Electromagnetic cascade in high-energy electron, positron, and photon interactions with intense laser pulses, Phys. Rev. A **87**, 062110 (2013).

[49] T. G. Blackburn, C. P. Ridgers, J. G. Kirk, and A. R. Bell, Quantum Radiation Reaction in Laser–Electron-Beam Collisions, Phys. Rev. Lett. **112**, 015001 (2014).

[50] D. G. Green and C. N. Harvey, Transverse Spreading of Electrons in High-Intensity Laser Fields, Phys. Rev. Lett. **112**, 164801 (2014).

[51] M. Vranic, J. L. Martins, J. Vieira, R. A. Fonseca, and L. O. Silva, All-Optical Radiation Reaction at 10^{21} W/cm^2, Phys. Rev. Lett. **113**, 134801 (2014).

[52] T. G. Blackburn, A. Ilderton, C. D. Murphy, and M. Marklund, Scaling laws for positron production in laser–electron-beam collisions, Phys. Rev. A **96**, 022128 (2017).

[53] M. Vranic, O. Klimo, G. Korn, and S. Weber, Multi-GeV electron-positron beam generation from laser-electron scattering, Sci. Rep. **8**, 4702 (2018).

[54] J. Magnusson, A. Gonoskov, M. Marklund, T. Zh. Esirkepov, J. K. Koga, K. Kondo, M. Kando, S. V. Bulanov, G. Korn, and S. S. Bulanov, Laser-Particle Collider for Multi-GeV Photon Production, Phys. Rev. Lett. **122**, 254801 (2019).

[55] C. N. Danson, C. Haefner, J. Bromage, T. Butcher, J.-C. F. Chanteloup, E. A. Chowdhury, A. Galvanauskas, L. A. Gizzi, J. Hein, D. I. Hillier *et al.*, Petawatt and exawatt class lasers worldwide, High Power Laser Sci. Eng. **7**, e54 (2019).

[56] V. Yakimenko, L. Alsberg, E. Bong, G. Bouchard, C. Clarke, C. Emma, S. Green, C. Hast, M. J. Hogan, J. Seabury, N. Lipkowitz, B. O'Shea, D. Storey, G. White, and G. Yocky, FACET-II facility for advanced accelerator experimental tests, Phys. Rev. Accel. Beams **22**, 101301 (2019).

[57] G. White and V. Yakimenko, On possible upgrades to FACET-II (private communication).

[58] G. White and V. Yakimenko, Ultra-short-*z* linear collider parameters, arXiv:1811.11782.

[59] A. R. Bell and John G. Kirk, Possibility of Prolific Pair Production with High-Power Lasers, Phys. Rev. Lett. **101**, 200403 (2008).

[60] A. M. Fedotov, N. B. Narozhny, G. Mourou, and G. Korn, Limitations on the Attainable Intensity of High Power Lasers, Phys. Rev. Lett. **105**, 080402 (2010).

[61] S. S. Bulanov, T. Zh. Esirkepov, A. G. R. Thomas, J. K. Koga, and S. V. Bulanov, Schwinger Limit Attainability

with Extreme Power Lasers, Phys. Rev. Lett. **105,** 220407 (2010).

[62] E. N. Nerush, I. Yu. Kostyukov, A. M. Fedotov, N. B. Narozhny, N. V. Elkina, and H. Ruhl, Laser Field Absorption in Self-Generated Electron-Positron Pair Plasma, Phys. Rev. Lett. **106,** 035001 (2011).

[63] N. V. Elkina, A. M. Fedotov, I. Yu. Kostyukov, M. V. Legkov, N. B. Narozhny, E. N. Nerush, and H. Ruhl, QED cascades induced by circularly polarized laser fields, Phys. Rev. ST Accel. Beams **14,** 054401 (2011).

[64] M. Jirka, O. Klimo, S. V. Bulanov, T. Zh. Esirkepov, E. Gelfer, S. S. Bulanov, S. Weber, and G. Korn, Electron dynamics and γ and e^- e^+ production by colliding laser pulses, Phys. Rev. E **93,** 023207 (2016).

[65] T. Grismayer, M. Vranic, J. L. Martins, R. A. Fonseca, and L. O. Silva, Laser absorption via quantum electrodynamics cascades in counter propagating laser pulses, Phys. Plasmas **23,** 056706 (2016).

[66] X.-L. Zhu, T.-P. Yu, Z.-M. Sheng, Y. Yin, I. C. E. Turcu, and A. Pukhov, Dense GeV electron-positron pairs generated by lasers in near-critical-density plasmas, Nat. Commun. **7,** 13686 (2016).

[67] M. Tamburini, A. Di Piazza, and C. H. Keitel, Laser-pulse-shape control of seeded QED cascades, Sci. Rep. **7,** 5694 (2017).

[68] A. Gonoskov, A. Bashinov, S. Bastrakov, E. Efimenko, A. Ilderton, A. Kim, M. Marklund, I. Meyerov, A. Muraviev, and A. Sergeev, Ultrabright GeV Photon Source via Controlled Electromagnetic Cascades in Laser-Dipole Waves, Phys. Rev. X **7,** 041003 (2017).

[69] T. Grismayer, M. Vranic, J. L. Martins, R. A. Fonseca, and L. O. Silva, Seeded QED cascades in counterpropagating laser pulses, Phys. Rev. E **95,** 023210 (2017).

[70] A. F. Savin, A. J. Ross, R. Aboushelbaya, M. W. Mayr, B. Spiers, R. H.-W. Wang, and P. A. Norreys, Energy absorption in the laser-QED regime, Sci. Rep. **9,** 8956 (2019).

[71] E. Cartlidge, The light fantastic, Science **359,** 382 (2018).

[72] J. Bromage, S.-W. Bahk, I. A. Begishev, C. Dorrer, M. J. Guardalben, B. N. Hoffman, J. B. Oliver, R. G. Roides, E. M. Schiesser, M. J. Shoup III *et al.*, Technology development for ultraintense all-OPCPA systems, High Power Laser Sci. Eng. **7,** e4 (2019).

[73] C. N. Danson, C. Haefner, J. Bromage *et al.*, Petawatt and exawatt class lasers worldwide, High Power Laser Sci. Eng. **7,** e54 (2019).

[74] R. G. Greaves and C. M. Surko, An Electron-Positron Beam-Plasma Experiment, Phys. Rev. Lett. **75,** 3846 (1995).

[75] B. D. Fried, Mechanism for instability of transverse plasma waves, Phys. Fluids **2,** 337 (1959).

[76] M. R. Edwards, N. J. Fisch, and J. M. Mikhailova, Strongly Enhanced Stimulated Brillouin Backscattering in an Electron-Positron Plasma, Phys. Rev. Lett. **116,** 015004 (2016).

[77] S. C. Wilks, J. M. Dawson, and W. B. Mori, Frequency Up-Conversion of Electromagnetic Radiation with Use of an Overdense Plasma, Phys. Rev. Lett. **61,** 337 (1988).

[78] K. Qu and N. J. Fisch, Laser frequency upconversion in plasmas with finite ionization rates, Phys. Plasmas **26,** 083105 (2019).

[79] M. R. Shcherbakov, K. Werner, Z. Fan, N. Talisa, E. Chowdhury, and G. Shvets, Photon acceleration and tunable broadband harmonics generation in nonlinear time-dependent metasurfaces, Nat. Commun. **10,** 1345 (2019).

[80] A. Nishida, N. Yugami, T. Higashiguchi, T. Otsuka, F. Suzuki, M. Nakata, Y. Sentoku, and R. Kodama, Experimental observation of frequency up-conversion by flash ionization, Appl. Phys. Lett. **101,** 161118 (2012).

[81] K. Qu, Q. Jia, M. R. Edwards, and N. J. Fisch, Theory of electromagnetic wave frequency upconversion in dynamic media, Phys. Rev. E **98,** 023202 (2018).

[82] M. R. Edwards, K. Qu, Q. Jia, J. M. Mikhailova, and N. J. Fisch, Cascaded chirped photon acceleration for efficient frequency conversion, Phys. Plasmas **25,** 053102 (2018).

[83] S. S. Bulanov, A. M. Fedotov, and F. Pegoraro, Damping of electromagnetic waves due to electron-positron pair production, Phys. Rev. E **71,** 016404 (2005).

[84] H. Peng, C. Riconda, S. Weber, C. T. Zhou, and S. C. Ruan, Frequency Conversion of Lasers in a Dynamic Plasma Grating, Phys. Rev. Applied **15,** 054053 (2021).

[85] W. L. Kruer, *The Physics of Laser Plasma Interactions* (Addison Wesley, Redwood City, 1988).

[86] E. Esarey, A. Ting, and P. Sprangle, Frequency shifts induced in laser pulses by plasma waves, Phys. Rev. A **42,** 3526 (1990).

[87] W. M. Wood, C. W. Siders, and M. C. Downer, Measurement of Femtosecond Ionization Dynamics of Atmospheric Density Gases by Spectral Blueshifting, Phys. Rev. Lett. **67,** 3523 (1991).

[88] T. D. Arber, K. Bennett, C. S. Brady, A. Lawrence-Douglas, M. G. Ramsay, N. J. Sircombe, P. Gillies, R. G. Evans, H. Schmitz, A. R. Bell *et al.*, Contemporary particle-in-cell approach to laser-plasma modelling, Plasma Phys. Controlled Fusion **57,** 113001 (2015).

[89] C. P. Ridgers, J. G. Kirk, R. Duclous, T. G. Blackburn, C. S. Brady, K. Bennett, T. D. Arber, and A. R. Bell, Modelling gamma-ray photon emission and pair production in high-intensity laser-matter interactions, J. Comput. Phys. **260,** 273 (2014).

[90] A. Gonoskov, S. Bastrakov, E. Efimenko, A. Ilderton, M. Marklund, I. Meyerov, A. Muraviev, A. Sergeev, I. Surmin, and E. Wallin, Extended particle-in-cell schemes for physics in ultrastrong laser fields: Review and developments, Phys. Rev. E **92,** 023305 (2015).

[91] M. Aicheler, P. Burrows, M. Draper, T. Garvey, P. Lebrun, K. Peach, N. Phinney, H. Schmickler, D. Schulte, and N. Toge, A multi-TeV linear collider based on CLIC technology: CLIC conceptual design report, Technical Report No. CERN Yellow Reports: Monographs (CERN, Geneva, 2012).

[92] A. Caldwell, K. Lotov, A. Pukhov, and F. Simon, Proton-driven plasma-wakefield acceleration, Nat. Phys. **5,** 363 (2009).

[93] J.-X. Li, K. Z. Hatsagortsyan, B. J. Galow, and C. H. Keitel, Attosecond Gamma-Ray Pulses via Nonlinear Compton Scattering in the Radiation-Dominated Regime, Phys. Rev. Lett. **115,** 204801 (2015).

[94] A. M. Fedotov, N. V. Elkina, E. G. Gelfer, N. B. Narozhny, and H. Ruhl, Radiation friction versus ponderomotive effect, Phys. Rev. A **90,** 053847 (2014).

[95] P. Flandrin, *Explorations in Time-Frequency Analysis* (Cambridge University Press, Cambridge, England, 2018).

[96] G. Thakur, E. Brevdo, N. S. Fučkar, and H.-T. Wu, The synchrosqueezing algorithm for time-varying spectral analysis: Robustness properties and new paleoclimate applications, Signal Processing **93**, 1079 (2013).

[97] I. Daubechies, J. Lu, and H.-T. Wu, Synchrosqueezed wavelet transforms: An empirical mode decomposition-like tool, Appl. Comput. Harmon. Anal. **30**, 243 (2011).

[98] D. J. Kane and R. Trebino, Characterization of arbitrary femtosecond pulses using frequency-resolved optical gating, IEEE J. Quantum Electron. **29**, 571 (1993).

[99] C. Iaconis and I. A. Walmsley, Spectral phase interferometry for direct electric-field reconstruction of ultrashort optical pulses, Opt. Lett. **23**, 792 (1998).